Magnetic Steering of Robotically Inserted Lateral-wall Cochlear-implant Electrode Arrays Reduces Forces on the Basilar Membrane In Vitro

*Cameron M. Hendricks, *Matt S. Cavilla, *David E. Usevitch, †Trevor L. Bruns, †Katherine E. Riojas, ‡Lisandro Leon, †Robert J. Webster III, §Frank M. Warren, and *Jake J. Abbott

Department of Mechanical Engineering, University of Utah, Salt Lake City, Utah; †Department of Mechanical Engineering, Vanderbilt University, Nashville, Tennessee; ‡Sarcos Robotics, Salt Lake City, Utah; and §The Oregon Clinic, Portland, Oregon

Hypothesis: Undesirable forces applied to the basilar membrane during surgical insertion of lateral-wall cochlear-implant electrode arrays (EAs) can be reduced via robotic insertion with magnetic steering of the EA tip.
Background: Robotic insertion of magnetically steered lateral-wall EAs has been shown to reduce insertion forces in vitro and in cadavers. No previous study of robot-assisted insertion has considered force on the basilar membrane.
Methods: Insertions were executed in an open-channel scala-tympani phantom. A force plate, representing the basilar membrane, covered the channel to measure forces in the direction of the basilar membrane. An electromagnetic source generated a magnetic field to steer investigational EAs with permanent magnets at their tips, while a robot performed the insertion.
Results: When magnetic steering was sufficient to pull the tip of the EA off of the lateral wall of the channel, it resulted in at least a 62% reduction of force on the phantom basilar membrane at insertion depths beyond 14.4 mm ($p < 0.05$), and these beneficial effects were maintained beyond approximately the same depth, even with 10 degrees of error in the estimation of the modiolar axis of the cochlea. When magnetic steering was not sufficient to pull the EA tip off of the lateral wall, a significant difference from the no-magnetic-steering case was not found.
Conclusions: This in vitro study suggests that magnetic steering of robotically inserted lateral-wall cochlear-implant EAs, given sufficient steering magnitude, can reduce forces on the basilar membrane in the first basilar turn compared with robotic insertion without magnetic steering.
Key Words: Cochlear implants—Magnetics—Robotics.

Otol Neurotol **42:**1022–1030, 2021.

Cochlear implants are neural-prosthetic devices in which an electrode array (EA) is placed inside the scala tympani (Fig. 1A) to provide electro-stimulation to the auditory nerve, enabling an otherwise deaf individual to hear. Unfortunately, the insertion of lateral-wall EAs can produce various forms of trauma due to scraping, folding, or buckling. This trauma may have a permanent effect on the patient, either reducing the quality of overall hearing, or in the worst case, causing loss of residual hearing. Although hearing loss can occur in many different ways, one of particular interest is perforation of the basilar membrane (Fig. 1B). Perforation can cause the endolymph and the perilymph within the scala media and scala tympani, respectively, to mix; if this occurs, any residual hearing of the patient will be lost (1). Early studies reported a basilar-membrane perforation rate of 25% with lateral-wall EAs (2,3), with the most common site of EA translocation being in the first basilar turn near 180 degrees (3–5). Although hearing preservation rates have increased due to advances in EA design, profound

Address correspondence and reprint requests to Jake J. Abbott, Ph.D., Department of Mechanical Engineering, University of Utah, 1495 E 100 S, 1550 MEK, Salt Lake City, UT 84112; E-mail: jake.abbott@utah.edu

Sources of support that require acknowledgment: Research reported in this publication was supported by the National Institute on Deafness and Other Communication Disorders of the National Institutes of Health under Award Number R01DC013168. The content is solely the responsibility of the authors and does not necessarily represent the official views of the National Institutes of Health.

Disclosures: J.J.A. has patents related to magnetic-field sources and magnetic steering of cochlear-implant electrode arrays.

Author Contributions: C.M.H. had full access to all of the data in the study and takes responsibility for the integrity of the data and the accuracy of the data analysis. Study concept and design: C.M.H., M.S.C., T.L.B., K.E.R., L.L., R.J.W., F.M.W., and J.J.A. Acquisition of data: C.M.H. and D.E.U. Analysis and interpretation of data: C.M.H., F.M.W., and J.J.A. Drafting of the Manuscript: C.M.H., D.E.U., and J.J.A. Critical revision of the manuscript for important intellectual content: All authors. Statistical Analysis: C.M.H. and D.E.U. Obtained funding: R.J.W., F.M.W., and J.J.A. Study supervision: J.J.A.

The authors disclose no conflicts of interest.

DOI: 10.1097/MAO.0000000000003129

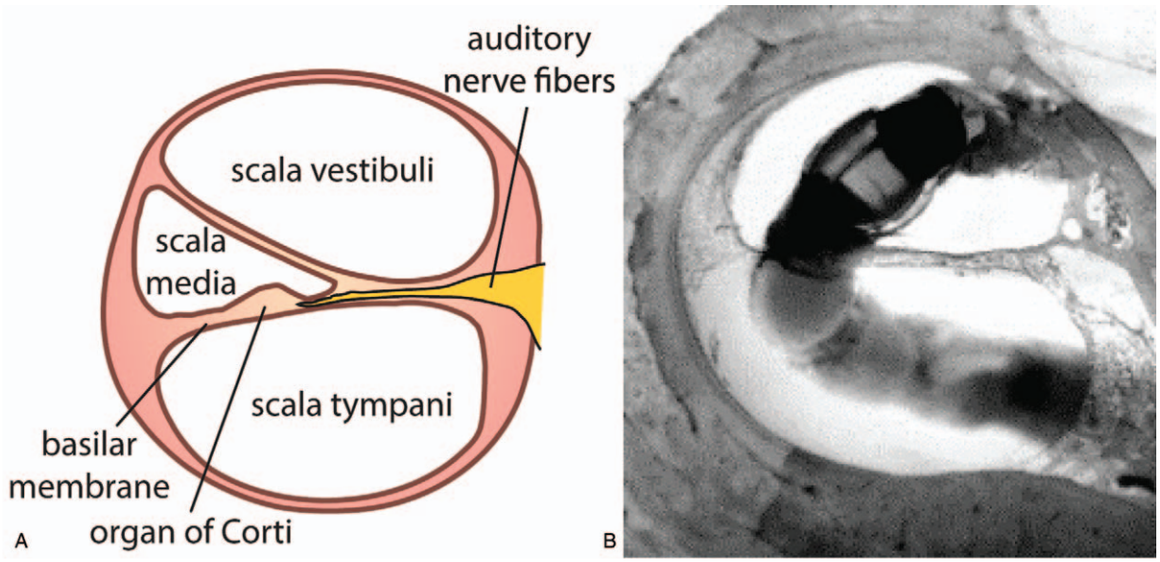

FIG. 1. *A*, Cross-section of the cochlea. *B*, Wardrop et al. (3) reported that the most typical injury found with the Nucleus banded lateral-wall EA was ''interscalar excursion.'' In the case illustrated here, a lateral-wall electrode array (EA) pierced the basilar membrane as it rounded the first turn of the cochlea near 180 degrees. The EA's tip bends back upon itself in the scala vestibuli and finally rests in the upper portion of the scala vestibuli with its tip facing the round window. Reprinted from Hearing Research, 203, Peter Wardrop, David Whinney, Stephen J. Rebscher, J. Thomas Roland, William Luxford, Patricia A. Leake, A temporal bone study of insertion trauma and intracochlear position of cochlear implant electrodes. I: Comparison of Nucleus banded and Nucleus Contour TM electrodes, 14, Copyright 2005, with permission from Elsevier.

loss of residual hearing is still as high as 11% (6–8). Hearing preservation is variable, and the causes of this variability is unknown (6), but it is understood that protection of the basilar membrane is critical to increasing hearing preservation rates (1). This is our motivation.

Multiple studies have been conducted involving robotic insertion of steerable EAs, with different methods of steering. Zhang et al. (9–11) found a 70% reduction in the insertion forces using robotic insertion combined with a tendon-based mechanically actuated steerable EA. Leon et al. (12) quantified insertion forces in vitro using multiple lateral-wall EA types, with and without steering, using magnetic torque as the method of steering. This was accomplished by adding a small permanent magnet to the tip of the EA, which was then actuated by a much larger external magnetic dipole source designed to reside adjacent to the patient's head, as originally proposed by Clark et al. (13). The magnetic torque steers the EA around the modiolus, and reduces insertion forces by keeping the tip of the EA off of the lateral wall and by generally reducing the pressure of the EA against the lateral wall. This result was recently replicated by Bruns et al. (14) in a cadaver cochlea. We employ this magnetic-steering method in this study.

Although those studies showed that steerable EAs reduce insertion forces, they do not consider which specific structures of the cochlea are protected, nor which structures might be placed at additional risk. From first principles, a reduction of insertion force must correspond to a net reduction in the forces applied by the EA against the walls of the cochlea. However, we are not aware of any studies that have considered the impact of robotic insertion, with or without steering, on the forces applied directly on the basilar membrane, which is arguably the most critical structure that can be damaged during the surgical insertion of the EA.

This study makes two contributions relative to the existing literature. The first is a custom scala-tympani phantom with a force-sensitive basilar membrane, for experiments characterizing insertion of cochlear-implant EAs. This setup enables basilar-membrane forces, as well as insertion forces, to be measured in vitro, which has not been possible previously. In the second contribution of this study, forces imparted on the phantom basilar membrane are compared between robotic insertions of lateral-wall EAs with and without magnetic steering. We demonstrate that magnetic steering significantly reduces forces on the basilar membrane, in spite of the fact that the magnetic steering does not explicitly account for the basilar membrane. This represents the first evidence that the addition of magnetic steering to robotically inserted EAs will help protect the basilar membrane, which is critical to maintaining residual hearing.

MATERIALS AND METHODS

To assess forces on the basilar membrane, an open-channel scala-tympani phantom was designed and fabricated. The scala-tympani model was based on the cochleostomy model of Leon et al. (15). The scala-tympani channel of that model was first arranged so that the modiolar axis was vertical (Fig. 2A). Then, the channel, which has an ascending-spiral geometry, was projected onto a horizontal plane and reduced to just 413

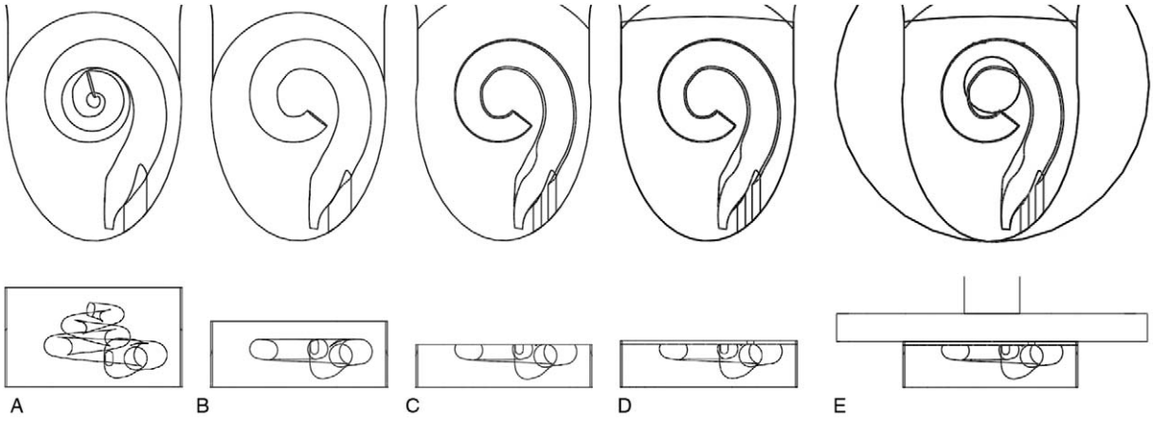

FIG. 2. Creation of scala-tympani phantom with force-sensitive basilar membrane. Top-down views are shown on the upper row, and front views are shown on the lower row. *A*, Full scala-tympani channel from the cochleostomy model of Leon et al. (15), with modiolar axis oriented vertically. *B*, Scala-tympani channel projected onto a horizontal plane, with angular reduction. *C*, Top of model removed to open channel. *D*, Thin plastic membrane attached to the top of model; membrane thickness enlarged for clarity. *E*, Force-plate sensor placed above the plastic membrane.

degrees to prevent the channel from intersecting with itself (Fig. 2B). These modifications enabled us to implement the force-sensitive basilar membrane, but also limited EA insertions to the first basilar turn, with a maximum insertion depth of 21 mm without reaching the end of the channel. Next, the top of the model was removed, creating an open scala-tympani channel (Fig. 2C). This phantom was fabricated using high-resolution stereolithography by Realize Inc. (Noblesville, IN). It is transparent for easy visualization.

The top of the phantom is then covered by a force-sensitive ceiling, which serves as the phantom basilar membrane that is contacted when the EA deviates upward from the channel. The phantom basilar membrane comprises two parts: a thin plastic membrane that directly covers the channel (Fig. 2D), and a high-resolution force sensor that is located above the plastic membrane (Fig. 2E). The plastic membrane is made of low-density polyethylene, with a thickness of 10 μm. Its purpose is to help trap the artificial perilymph that fills the channel, and to eliminate any surface tension between the artificial perilymph and the force sensor. In preliminary testing it was found that surface tension between the force sensor and the phantom scala tympani would cause unreliable readings; the inclusion of the thin plastic membrane eliminated this problem. The force sensor used is a custom calibrated capacitance-based one-degree-of-freedom sensor fabricated by Nanodyne Measurement Systems (Minneapolis, MN). The measured forces represent the integration of all basilar-membrane forces distributed along the length of the inserted EA. The sensor can measure up to 147 mN with a resolution of 2.25 μN, which is a much higher resolution than sensors that have been used in previous works to measure EA insertion forces.

Due to the inclusion of the plastic membrane over the channel, the values measured by the force sensor may not fully capture the total applied force of the EA. In fact, we assume from first principles that the force sensor will underestimate the applied force of the EA, since the plastic membrane will support some portion of the applied force. However, in this study, we are not particularly interested in measuring the absolute value of the forces imparted on the basilar membrane. Rather, we are interested in the relative reduction in forces due to magnetic steering.

During preliminary testing, it was discovered that alignment of the planar upper surface of the scala-tympani phantom with the planar force plate would require high precision to record reliable data, as preloading the sensor orthogonal to its intended sensing direction would result in sensor drift. As a result, a custom robotic alignment system was designed and constructed (Fig. 3), which enables the scala-tympani phantom to be moved up into position beneath the stationary force sensor. This robotic system enables independent control over the vertical height of its end-effector, on which the scala-tympani phantom is mounted, as well as the direction of its surface normal.

Alignment of the scala-tympani phantom was performed as follows. The plastic membrane was placed over top of the phantom. Then the phantom was raised up to the force plate such that the two surfaces were approximately parallel and nearly touching. Then the phantom was raised using one of the three stages until a force was read by the force sensor, at which point the stage was backed off (i.e., lowered) until only a slight force was detected. This process was repeated for each of the three stages sequentially until advancing any of the stages farther would cause an increase in force, at which point the sensor was zeroed. The final result is a phantom that is preloaded slightly ($\leq$3 mN) with the sensor. Note that, with the given preload and zeroing of the sensor, it is possible for the force measurements to take on negative values in cases in which the EA pushes downward on the scala-tympani phantom, resulting in a reduction in the preload between the scala-tympani phantom and the force plate due to a small amount of compliance in the alignment system. Because our study is focused on basilar-membrane forces and not scala-tympani forces, and since there is no physical mechanism for the EA to apply tension forces on the basilar membrane, any negative force readings were recorded as zero.

During preliminary testing, it was found that bubbles in the channel would affect the path of the EA, forcing it into the scala-tympani walls. To mitigate this phenomenon, a small hole was drilled at the end of the scala-tympani channel and a tube was attached to this small hole. The other end of the tube was connected to a syringe filled with the artificial perilymph. This system was used to add fluid to the channel between tests, which removed any bubbles.

The system that we used for robotic insertion of EAs, with and without magnetic steering, is a copy of the system recently described by Bruns et al. (14). The system comprises two

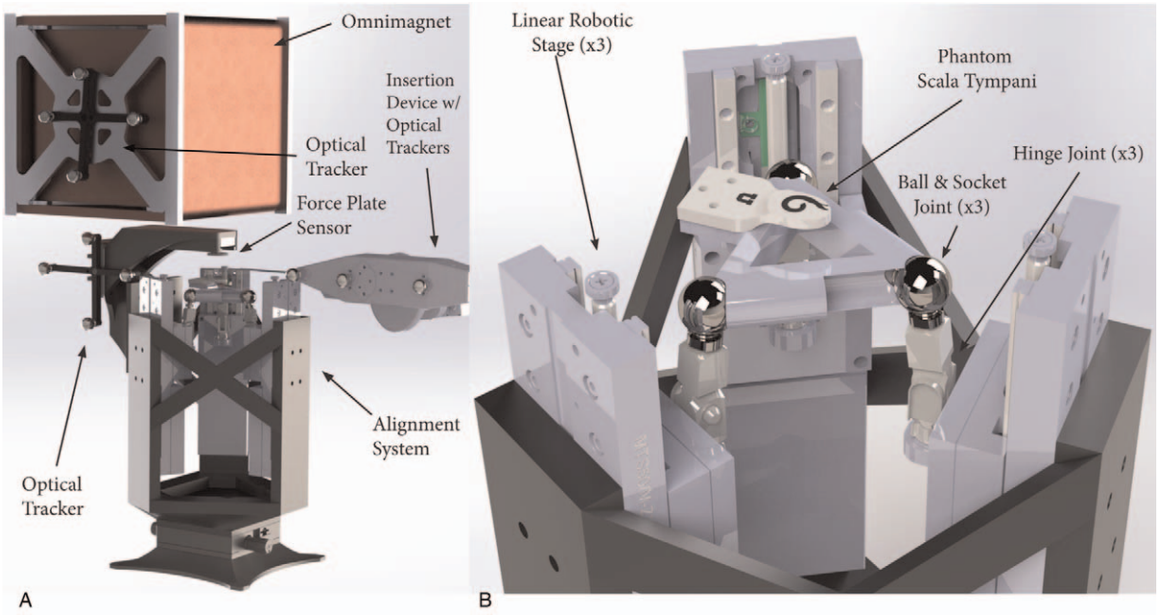

FIG. 3. *A*, Rendering of complete experimental system. *B*, Rendering of robotic system for precision alignment of the scala-tympani phantom with respect to the force plate.

principal components: a robotic insertion device, and an Omnimagnet electromagnetic field source. Renderings of the complete system integrated with the force-sensitive phantom cochlea are shown in Figure 3A. All subsystems are integrated and controlled using software written in C++, with a sampling rate of 1000 Hz. The software controls the insertion velocity (1.3 mm/s) and corresponding depth of the EA, as well as the electrical current commands to the Omnimagnet. It also performs the magnetic-field computations required to calculate the electrical current commands. Finally, it records the forces applied to the plate sensor. The center of the Omnimagnet was placed along the unit vector $\hat{p} = [0.98 \quad 0.21 \quad -0.05]^T$, measured with respect to the center of the cochlea, which represents the optimal direction of the external magnetic source with respect to the cochlea defined by Leon et al. (16). To reduce power requirements, the Omnimagnet needs to be as close to the cochlea as possible. The final position of the Omnimagnet for all insertions in this study is $\hat{p} = [117 \quad 25 \quad -6]^T$ mm, measured with respect to the center of the cochlea. This Omnimagnet position is closer than the distance that will be required in a clinical system. This compromise was due to limitations of the system's magnetic field. The result of being too close is that magnetic force, which tends to pull the magnetic tip of the EA upward into the phantom basilar membrane (as opposed to the magnetic torque that is being used for steering) is larger than what it would be in a clinical system. Consequently, the results of our study will be conservative, since we are interested in reducing forces on the basilar membrane using magnetic steering.

To enable magnetic steering, two different magnetically tipped EAs were fabricated by modifying MED-EL Standard (31.5 mm in length) EAs (Fig. 4). Both of the EAs used grade-N52 NdFeB magnets. The EA with the smaller magnetic dipole contained two axially magnetized cylindrical permanent magnets that were connected axially and embedded in silicone at the tip of the EA. Each of the individual magnets had a diameter of 0.3 mm and a length of 0.5 mm, resulting in a total dipole moment of $||\vec{m}|| = 3.33 \times 10^{-4} \mathrm{A} \cdot \mathrm{m}^2$. The EA with the larger magnetic dipole was fabricated by attaching a single axially magnetized cylindrical permanent magnet to the tip of the EA via an anchor. This anchor was over-molded into the cochlear implant to provide a flat cylindrical surface for the magnet to attach. The magnet had a diameter of 0.5 mm and a length of 1 mm, resulting in a total a dipole moment of $|| \rightarrow || = 9.25 \times 10^{-4} \mathrm{A} \cdot \mathrm{m}^2$. That is, a 67% increase in the EA magnet's diameter resulted in a 178% increase in the magnet's volume and strength.

The magnetic torque $\vec{\tau} = \vec{m} \times \vec{b}$ (units N·m) is due to the cross product of the dipole moment of the EA permanent magnet and the magnetic field, $\vec{b}$ (units T). To generate the largest torque possible with a magnetic field of a given strength, the magnetic field is directed perpendicular to the dipole moment (i.e., the cylindrical axis of the permanent magnet). Before insertion, paths are generated, corresponding to the position of the tip of the EA at each insertion depth (Fig. 5). The path used for these experiments was created by Cohen et al. (17), with a small modification described by Clark et al. (18). This path approximates the resting position of the EA in our scala-tympani phantom. These path points are then associated with the desired magnetic field corresponding to each insertion depth.

We use a repeated-measures experimental design to characterize force on the basilar membrane using one treatment variable and one blocking variable. The treatment variable (EA Type) has three levels: nonmagnetic, small magnet, and large magnet. The blocking variable (EA Rotation), which is included to mitigate potential confounding factors related to any plastic deformation of the EAs after repeated insertion, has four levels of rotation about the EA's central axis at the proximal end: 0 degree, 90 degrees, 180 degrees, and 270 degrees. Insertion experiments were separated into three blocks, with each block comprising three sequential insertions at each of the four levels of EA Rotation—with order chosen at random,

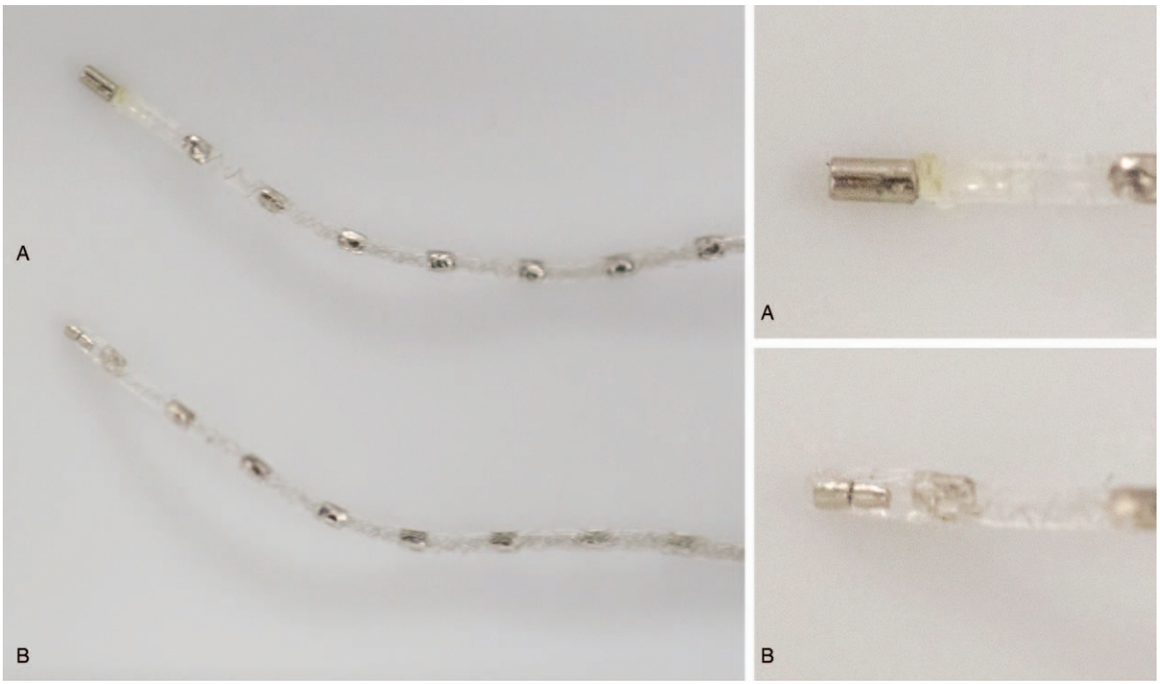

FIG. 4. Magnetically tipped electrode arrays used in experiments. *A*, Large magnet attached to tip. *B*, Small magnets embedded in tip.

without replacement—for each of the three levels of EA Type. This resulted in 36 total insertions for each level of EA Type.

Under the conjecture that magnetic steering may do more harm than good if it is not being applied in the correct direction, we subsequently conducted four more experiments to characterize the effect of an error in our estimate of the modiolar axis (which is parallel to the *x* axis in Fig. 5). Each of these four experiments considered a rotational error of 10 degrees in one of four directions: about the *y* axis and *z* axis in each of the positive and negative directions. Each of these four experiments were designed similar to our principal experiment described above, but with three differences: only one level of EA Type was considered (large magnet), only three values of EA Rotation were considered (0 degree, 90 degrees, and 180 degrees), and only one block of data was collected. This resulted in three total insertions for each type of modiolar-axis error. The rationale for only considering large-magnet EAs was based upon the results observed in the principal experiment. The rationale for

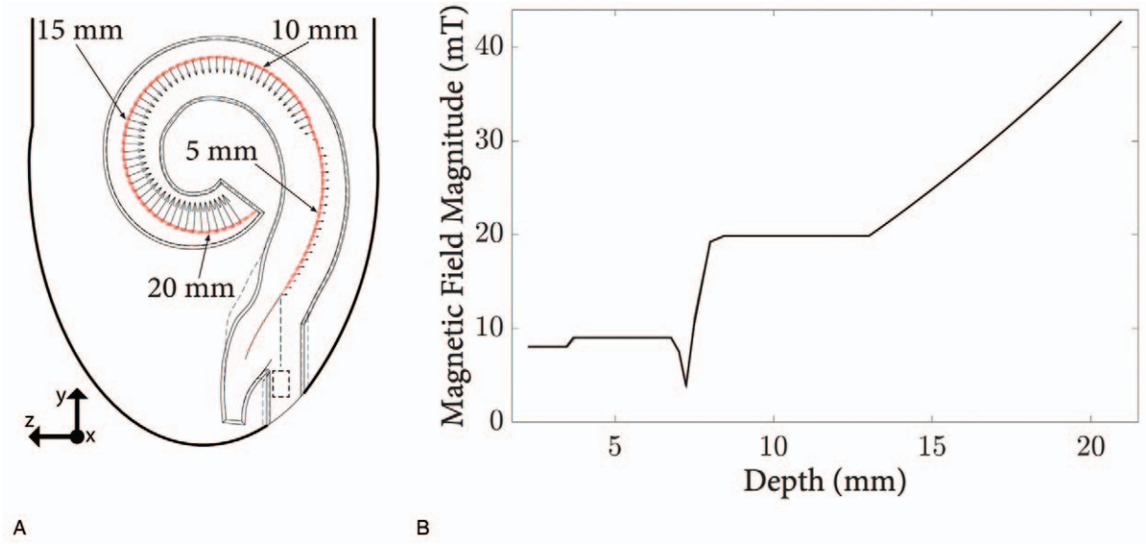

FIG. 5. Magnetic steering of the electrode arrays. *A*, Precomputed path. The magnetic-steering field, $\vec{b}$, is indicated by black *arrows*. Red *arrows* define the tangent vectors of the path. The dotted *line* defines the portion of path without any magnetic steering. *B*, Magnitude of magnetic field, $||\vec{b}||$, versus insertion depth.

performing fewer insertion trials was that our EAs began to accumulate plastic deformation, and we did not need to collect more data to observe statistically significant results.

It should be noted that, although modiolar-axis estimation error is likely to be the main source of magnetic-steering error, other potential sources of error include error in the position estimate of the cochlea relative to the external magnetic-field source, calibration error of the external magnetic-field source, or misalignment of the permanent magnet attached to the tip of the EA. However, our choice of 10 degrees modiolar-axis error was designed to be robust to approximate some of these other sources of error. In clinical practice, a CT scan of the patient can be used to estimate the modiolar axis (19,20), and the most recent and most effective of these methods results in an average error of only 2.5 degrees (20).

During the insertion experiments, the phantom cochlea was covered with the thin plastic membrane and the phantom cochlea was aligned with the force sensor. The force sensor was zeroed and artificial perilymph was then pumped into the cochlea. The EA of choice was then loaded into the insertion device. A Polaris Spectra optical tracking system was used to place the Omnimagnet and insertion device relative to the phantom cochlea. The optical-tracking markers can be seen in Figure 3A. The Omnimagnet was aligned first, followed by a coarse alignment of the insertion device using an articulating arm. These alignments were both done using only the Polaris Spectra optical tracking system. All positioning was done to an accuracy of 1.5 mm and 3 degrees when using the Polaris Spectra. A fine alignment was then performed with the Newport three-degrees-of-freedom linear stage. This fine alignment was done using visual feedback from the digital microscope, which can be seen in Figure 3B. The starting point for the tip of each EA is shown by the dashed box shown in Figure 5A.

Three blocks of data were collected during testing. Each block of data consisted of 12 insertions total for each EA type (nonmagnetic, small magnet, large magnet), for a total of 36 insertions for each EA type ($n = 36$) in the study. Within each block, insertions with the large-magnet EAs were performed first, followed by small-magnet and nonmagnetic insertions. Small-magnet and nonmagnetic insertion sets took place consecutively since the same EA was used for these two types of insertion, alternating which EA type was done first. The 12 insertions per EA type were further divided into rotations about the central axis of the EA (0 degree, 90 degrees, 180 degrees, and 270 degrees). These four rotations were chosen randomly without replacement. Dividing the 12 insertions by four unique rotations resulted in three insertions per rotation; these three insertions were done consecutively and are defined as an insertion set.

To reduce high-frequency noise in the force data, all data collected was post-processed with a moving-average filter with a window size of 50 (i.e., 50 ms). Some of the insertions induced buckling of the portion of the EA that was outside of the scala-tympani channel. If this occurred, the insertion would be stopped prematurely to ensure that no major plastic deformation of the EA would occur, and the EA would be straightened out by hand.

Additional details about this study can be found in Hendricks (21).

RESULTS

The results for the principal experiment are shown in Figure 6A, with results depicted as mean basilar-membrane forces with 95% confidence intervals as a function of insertion depth (measured from the cochleostomy opening). We find that the large-magnet EA results in at least a 62% reduction in force compared with the nonmagnetic EA for depths of approximately 14.4 mm and beyond ($p < 0.05$); the effect size as a function of depth is shown in Figure 6F. The difference in force becomes more pronounced with increasing insertion depth. We do not find a significant reduction in basilar-membrane force when using the small-magnet EA, at any depth.

The results for the four experiments in which we consider 10 degrees errors in the estimation of the modiolar axis are shown in Figure 6B–E. Recall that we only consider the large-magnet EA here, due to the poor performance of the small-magnet EA in the previous experiment. Note that the confidence intervals here are quite wide due to the limited number of trials. However, even accounting for this, we still find a significant reduction in force ($p < 0.05$) for depths of approximately 17 mm (conservatively) and beyond, with effect sizes as a function of depth shown in Figure 6F.

DISCUSSION

The results for our principal experiment, depicted in Figure 6A, indicate that there was not a significant reduction in basilar-membrane force when using the small-magnet EA compared with nonmagnetic insertions at any depth. This result is not trivial considering that we would expect to see a reduction in insertion force for this case (12). With the small-magnet EA, a portion of the torque required to bend the EA, which is naturally straight, is being provided by the magnetic steering. As a result, the forces being applied by the walls of the scala tympani are necessarily less; this is the cause of the reduction in insertion force. However, with the small-magnet EA we did not observe the tip of the EA leaving the walls of the scala tympani, whereas we did observe the tip of the large-magnet EA leave the walls of the scala tympani. This suggests that, although any amount of magnetic steering will provide some reduction in insertion force, for the reduction of forces on the basilar membrane it is important to generate enough magnetic torque to cause the tip of the EA to move away from the walls of the scala tympani (at least in the critical first basilar turn in which damage to the basilar membrane is most likely to occur).

The magnetic-steering system used has a current limit of 30 A continuous and 50 A peak. During all magnetic insertions, the system was configured to use as much current as possible by the end of the insertion, where the radius of curvature is the smallest. Because magnetic torque is the product of the strength of the magnetic field and the strength of the embedded permanent magnet, it is possible to get the same results from this study with the smaller embedded magnet as long as the magnetic torque is unchanged. This would either involve using an Omnimagnet that can source more current (and dissipate the associated heat) more effectively by adding cooling,

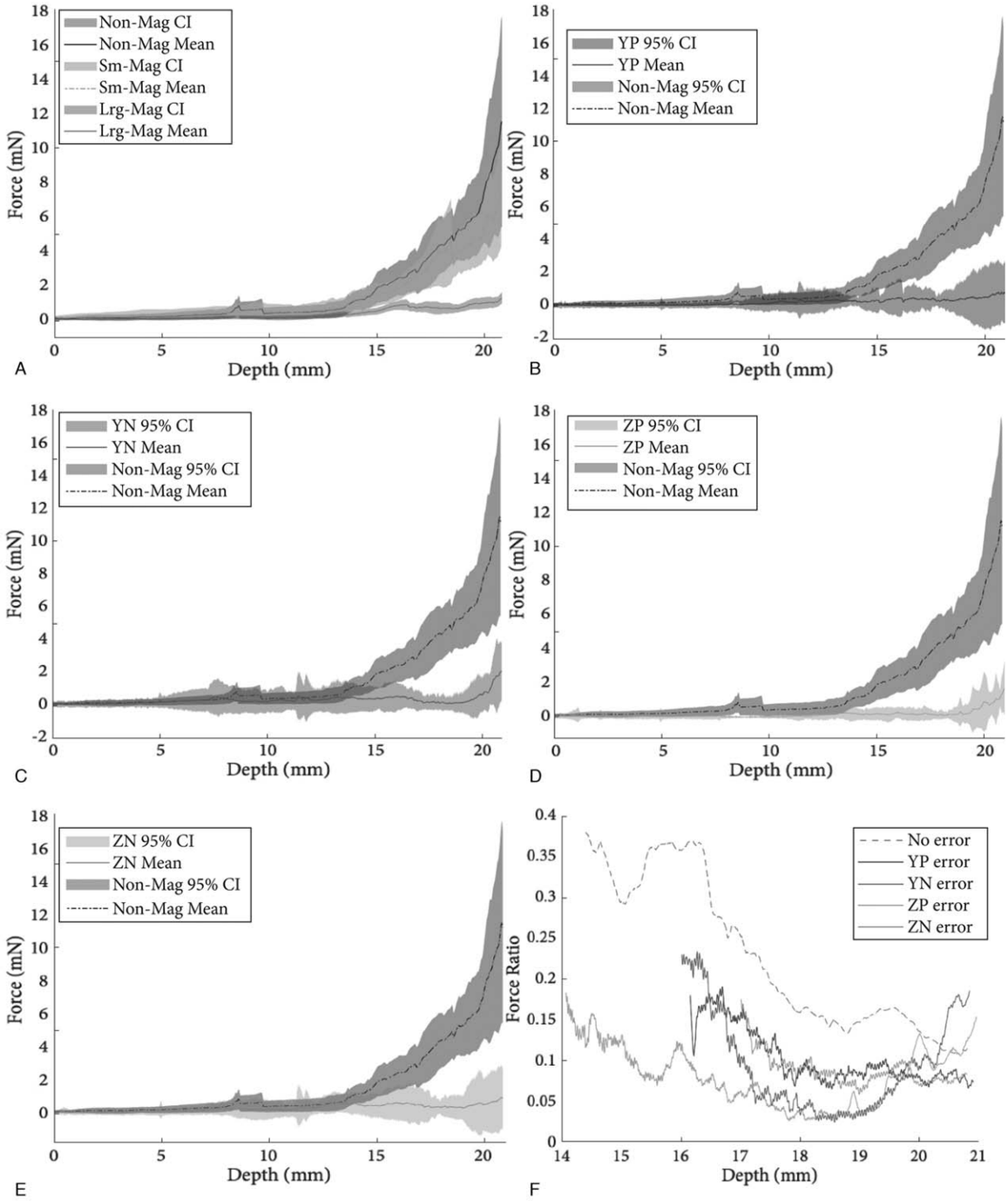

FIG. 6. Force on the phantom basilar membrane as a function of insertion depth, shown as a mean with 95% confidence interval. *A*, Principal insertion experiment (n = 36). *B–E*, Insertion experiments with the large-magnetic electrode array (EA) with 10 degrees of error in magnetic steering (n = 3) for (*B*) error about the positive *y* axis, (*C*) error about the negative *y* axis, (*D*) error about the positive *z* axis, and (*E*) error about the negative *z* axis. *F*, Ratio of the mean basilar-membrane force with the large-magnet EA to the mean basilar-membrane force with the nonmagnetic EA, for each of the five cases tested, shown in the region where significant differences were observed ($p < 0.05$).

using a larger Omnimagnet, or using a permanent magnet as the external source.

Our insertions were all performed at a speed of 1.3 mm/s, which is the same value used in our recent study with the same system (14). This speed avoided excessive heating in the Omnimagnet while also avoiding any buckling in the EA, but it is not necessarily optimal. For reference, manual insertions are typically performed in the range of 0.87 to 1.6 mm/s (22), and robotic insertions have been performed across a wider range of 0.025 to 7.5 mm/s (9,23–27), with evidence suggesting that insertions should be slow and steady for best clinical outcomes (28,29), and with some evidence that going too slow could actually be counterproductive (26).

In this study, the EA magnets were permanently attached, but in practice we would not want to leave a permanent magnet inside the patient after the insertion, due to problems with magnetic resonance imaging (MRI) compatibility. We are currently pursuing strategies to rigidly attach the magnet on the inner side of the EA tip, such that it can be released and removed after insertion. The oblong cross-section of the scala typani (see Fig. 1) suggests that space exists for such a concept to be successful. Because we are utilizing magnetic torque for steering, as opposed to magnetic force, the steering is insensitive to a lateral shift of the EA magnet.

This study provides the first compelling evidence that magnetic steering of robotically inserted EAs will reduce forces on the basilar membrane in the first basilar turn, which is critical to protecting the basilar membrane and retaining residual hearing with cochlear implants, although in vivo testing is still required. The strength and optimal placement of the Omnimagnet for clinical use is described by Leon et al. (16), and the process for image-guided alignment of the Omnimagnet and the robotic insertion device with respect to the patient, and using patient-specific plans based on preoperative computed tomography (CT) scans, is already described in Bruns et al. (14).

Acknowledgments: The authors gratefully acknowledge support from Dr. Anandhan Dhanasingh of MED-EL for fabricating the small-magnet electrodes used in this study.

REFERENCES

1. Wanna GB, Noble JH, Gifford RH, et al. Impact of intrascalar electrode location, electrode type, and angular insertion depth on residual hearing in cochlear implant patients: preliminary results. *Otol Neurotol* 2015;36:1343–8.
2. Ketten DR, Skinner MW, Wang G, et al. In vivo measures of cochlear length and insertion depth of nucleus cochlear implant electrode arrays. *Ann Otol Rhinol Laryngol Suppl* 1998;107: 1–16.
3. Wardrop P, Whinney D, Rebscher SJ, et al. A temporal bone study of insertion trauma and intracochlear position of cochlear implant electrodes. I: Comparison of Nucleus banded and Nucleus Contour^{TM} electrodes. *Hear Res* 2005;203:54–67.
4. Nguyen Y, Miroir M, Kazmitcheff G, et al. Cochlea implant insertion forces in microdissected human cochlea to evaluate a prototype array. *Audiol Neurotol* 2012;17:290–8.
5. Torres R, Drouillard M, De Seta D, et al. Cochlear implant insertion axis into the basal turn: a critical factor in electrode array translocation. *Otol Neurotol* 2018;39:168–76.
6. Moran M, Dowell RC, Iseli C, et al. Hearing preservation outcomes for 139 cochlear implant recipients using a thin straight electrode array. *Otol Neurotol* 2017;38:678–84.
7. Pillsbury HC III, Dillon MT, Buchman CA, et al. Multicenter US clinical trial with an electric-acoustic stimulation (EAS) system in adults: final outcomes. *Otol Neurotol* 2018;39:299–305.
8. Skarzynski PH, Skarzynski H, Dziendziel B, et al. Hearing preservation with the use of Flex20 and Flex24 electrodes in patients with partial deafness. *Otol Neurotol* 2019;40:1153–9.
9. Zhang J, Bhattacharyya S, Simaan N. Model and parameter identification of friction during robotic insertion of cochlear-implant electrode arrays.*Paper Presented at: IEEE International Conference on Robotics and Automation*. 2009. 3859–3864.
10. Zhang J, Wei W, Ding J, et al. Inroads toward robot-assisted cochlear implant surgery using steerable electrode arrays. *Otol Neurotol* 2010;31:1199–206.
11. Zhang J, Xu K, Simaan N, et al. A pilot study of robot-assisted cochlear implant surgery using steerable electrode arrays. *Paper Presented at: International Conference on Medical Image Computing and Computer-Assisted Intervention*. 2006. 33–40.
12. Leon L, Warren FM, Abbott JJ. An in-vitro insertion-force study of magnetically guided lateral-wall cochlear-implant electrode arrays. *Otol Neurotol* 2018;39:e63–73.
13. Clark JR, Leon L, Warren FM, et al. Magnetic guidance of cochlear implants: proof-of-concept and initial feasibility study. *J Med Dev* 2012;6:035002.
14. Bruns TL, Riojas KE, Ropella DS, et al. Magnetically steered robotic insertion of cochlear-implant electrode arrays: system integration and first-in-cadaver results. *IEEE Robot Automat Lett* 2020;5:2240–7.
15. Leon L, Cavilla MS, Doran MB, et al. Scala-tympani phantom with cochleostomy and round-window openings for cochlear-implant insertion experiments. *J Med Dev* 2014;8:041010.
16. Leon L, Warren FM, Abbott JJ. Optimizing the magnetic dipole-field source for magnetically guided cochlear-implant electrode-array insertions. *J Med Robot Res* 2018;3:1850004.
17. Cohen LT, Xu J, Xu SA, et al. Improved and simplified methods for specifying positions of the electrode bands of a cochlear implant array. *Am J Otol* 1996;17:859–65.
18. Clark JR, Warren FM, Abbott JJ. A scalable model for human scala-tympani phantoms. *J Med Dev* 2011;5:014501.
19. Demarcy T, Vandersteen C, Guevara N, et al. Automated analysis of human cochlea shape variability from segmented μCT images. *Comput Med Imaging Graph* 2017;59:1–12.
20. Wimmer W, Vandersteen C, Guevara N, et al. Robust cochlear modiolar axis detection in CT.*Paper Presented at: International Conference on Medical Image Computing and Computer-Assisted Intervention*. 2019.
21. Hendricks CM. *An In-vitro Study of Forces on the Basilar Membrane During Magnetically Steered Robotic Insertion of Lateral-wall Cochlear-implant Electrode Arrays*. Department of Mechanical Engineering, University of Utah, Salt Lake City, Utah; 2020. Master's Thesis.
22. Kesler K, Dillon N P, Fichera L, et al. Human kinematics of cochlear implant surgery: an investigation of insertion micromotions and speed limitations. *Otolaryngol Head Neck Surg* 2017;157:493–8.
23. Majdani O, Schurzig D, Hussong A, et al. Force measurement of insertion of cochlear implant electrode arrays in-vitro: comparison of surgeon to automated insertion tool. *Acta Otolaryngol* 2010;130:31–6.
24. Pile J, Simaan N. Characterization of friction and speed effects and methods for detection of cochlear implant electrode tip fold-over.-*Paper Presented at: IEEE International Conference on Robotics and Automation*. 2013. 4409–4414.
25. Banakis Hartl RM, Kaufmann C, Hansen MR, et al. Intracochlear pressure transients during cochlear implant electrode insertion:

effect of micro-mechanical control on limiting pressure trauma. *Otol Neurotol* 2019;40:736–44.
26. Kaufmann CR, Henslee AM, Claussen A, et al. Evaluation of insertion forces and cochlea trauma following robotics-assisted cochlear implant electrode array insertion. *Otol Neurotol* 2020; 41:631–8.
27. Hügl S, Rülander K, Lenarz T, et al. Investigation of ultra-low insertion speeds in an inelastic artificial cochlear model using custom-made cochlear implant electrodes. *Eur Arch Otorhinolaryngol* 2018;275:2947–65.
28. Kontorinis G, Lenarz T, Stöver T, et al. Impact of the insertion speed of cochlear implant electrodes on the insertion forces. *Otol Neurotol* 2011;32:565–70.
29. Rajan GP, Kontorinis G, Kuthubutheen J. The effects of insertion speed on inner ear function during cochlear implantation: a comparison study. *Audiol Neurotol* 2013;18:17–22.